Loop-Shaping Method with Unstable Poles for Magnetic-Head Positioning Control in Hard Disk Drive

Takenori Atsumi
Department of Mechanical Engineering
Chiba Institute of Technology
Narashino, Japan
takenori.atsumi@p.chibakoudai.jp

Shota Yabui
Department of Mechanical Systems Engineering
Tokyo City University
Tokyo, Japan
yabuis@tcu.ac.jp

Atsushi Okuyama
Department of Precision Engineering
Tokai University
Hiratsuka, Japan
okuyama@tokai-u.jp

Masahiro Mae
Department of Electrical Engineering and Information Systems
The University of Tokyo
Tokyo, Japan
mmae@ieee.org

***Abstract*—In this paper, we present a loop-shaping method that incorporates unstable poles for the magnetic-head positioning system in a hard disk drive (HDD). The proposed method involves introducing unstable poles instead of the conventional stable poles for the resonance filter used in loop shaping. In our approach, the resonant filter is designed to realize a circle that includes the coordinate $[-1, 0j]$ on the Nyquist plot of the open-loop characteristics in the control system. Validation results using the HDD benchmark problem demonstrate that our proposed methods effectively reject disturbances in the high-frequency range while maintaining robust performance.**

***Index Terms*—Resonant Filter, Unstable Pole, Loop Shaping, Hard Disk Drives, Positioning Control**

I. Introduction

The future of cloud services relies on the expansion of hard disk drive (HDD) capacity, as data demands within cloud services are growing rapidly. To address this challenge, we aim to enhance the precision of magnetic-head positioning control systems, which will ultimately reduce the bit size required for data storage on a disk.

In magnetic-head positioning control systems, a significant obstacle to improving positioning accuracy is the presence of mechanical oscillations in the high-frequency range. Overcoming this disturbance proves complex because the oscillation frequency often exceeds the servo bandwidth of the control system or the resonant frequencies of the controlled components.

To tackle this issue, we have proposed loop-shaping methods that incorporate resonant filters. These methods allow us to effectively suppress disturbances occurring beyond the servo bandwidth and the mechanical resonant frequencies [1], [2]. In this paper, we present a loop-shaping method that introduces unstable poles for the resonant filters. We validate this approach using the HDD benchmark problem, demonstrating its applicability to the latest HDDs.

A part of this work is supported by JSPS KAKENHI Grant Number JP22K04170.

II. Loop-shaping method with resonant filter

The loop-shaping is widely used for improving the positioning accuracy for stable control systems [3]–[11]. In this paper, we employ resonant filters to improve the stable control system based on the loop-shaping scheme.

A. Principle of resonant filter (conventional method)

In this study, the frequency response of $G[z]$ at ω [rad/s] is expressed as $G[e^{j\omega T_s}]$, where T_s represents the sampling time of $G[z]$. We have made the assumption that a similar representation holds for the frequency response of an unstable system.

A control system design with the resonant filter enables us to add a phase-stable circle in a vector locus of the open-loop characteristics of the control system so that the gain of sensitivity function $|S[z]|$ decreases at the disturbance's frequency [1]. In this method, a resonant mode R_0 is given as

$$R_0(s) = \frac{\kappa_r}{s^2 + 2\zeta_r\omega_r s + {\omega_r}^2}, \tag{1}$$

where κ_r is the modal gain, ζ_r is the damping ratio, and ω_r is the resonance frequency. In order to decrease the gain of the sensitivity function, we employ a resonant filter $R[z]$ which is discretized $R_c(s)$:

$$R_c(s) = R_0(s)C_r(s), \tag{2}$$

where C_r is a phase compensator.

Fig. 1 shows the principle of the resonant filter. Here, $[a_r, b_r j]$ means a coordinate of the open-loop characteristic

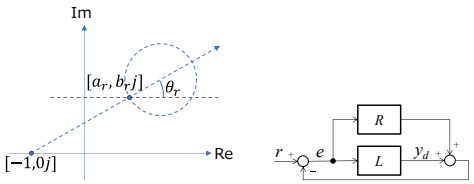

(a) Vector locus of resonant filter (b) Block diagram

Fig. 1. Principle of resonant filter

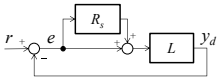

Fig. 2. Block diagram with resonant filter.

L at a target frequency of the resonant filter (the resonant frequency of the resonant filter). The resonant filter is designed so as to add a circle that makes the vector locus away from the $[-1, 0j]$ like Fig. 1 (a). To do so, the phase of the resonant filter should be

$$\angle R[e^{j\omega_r T_s}] = \theta_r, \tag{3}$$

where

$$\theta_r = \arctan\left(\frac{b_r}{a_r + 1}\right). \tag{4}$$

To realize the circle, we should add a phase-stable resonant filter R in parallel connection to L like Fig. 1 (b). However, this control system is not able to reject the disturbance because the output signal of the resonant filter is added to the control variable after adding the disturbance. Therefore, to reject the disturbance, the resonant filter R_s is added in series connection to L like Fig. 2. $R_s[z]$ can be given as the discretized $R_{sc}(s)$:

$$R_{sc}(s) = \frac{R_0(s)C_r(s)}{\tilde{L}(s)}, \tag{5}$$

where $\tilde{L}$ is approximated L around ω_r (the resonant frequency of R). Note that $\tilde{L}$ does not include unstable zeros. The phase of the resonant filter at ω_r should be

$$\angle R_s[e^{j\omega_r T_s}] = \theta_r - \angle L[e^{j\omega_r T_s}]. \tag{6}$$

In this paper, as discretization method for the resonant filters, we employ the Bilinear (Tustin) method with frequency pre-warping at ω_r.

To reject multiple disturbances, we can employ multiple resonant filters as follows,

$$R_s[z] = \sum_{m=1}^{M_d} R_{sm}[z, m], \tag{7}$$

where M_d is the number of target disturbances, and R_{sm} is the resonant filter for each disturbance.

B. Resonant filter with unstable poles (proposed method)

In the resonant filter scheme, we are able to employ unstable poles instead of stable poles. Similar to resonance characteristics using stable poles, resonance characteristics

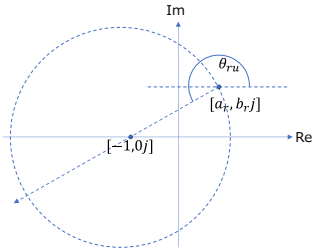

Fig. 3. Vector locus of a resonant filter with unstable poles.

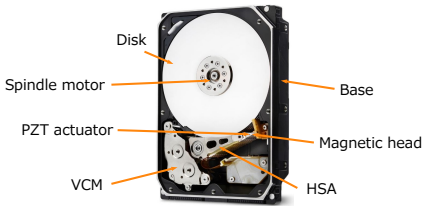

Fig. 4. Hard disk drive.

achieved by unstable poles trace circular paths on the Nyquist plot. However, their direction is counterclockwise in vector trajectory.

According to the Nyquist stability criterion, the control system is stable when the circle realized by the resonant filter with unstable poles includes the coordinate $[-1, 0j]$ on the Nyquist plot of the open-loop characteristics. Therefore, in order to decrease the gain of the sensitivity function, the resonant filter with the unstable pole is designed so as to add a circle which makes the vector locus like Fig. 3. Therefore, in the case of the unstable poles, the phase of the resonant filter at ω_r should be

$$\angle R_s[e^{j\omega_r T_s}] = \theta_{ru} - \angle L[e^{j\omega_r T_s}], \tag{8}$$

where,

$$\theta_{ru} = \arctan\left(\frac{b_r}{a_r + 1}\right) + \pi. \tag{9}$$

Note that the resonant filter with unstable poles must have a large gain to contain the coordinates $[-1, 0j]$ inside the circle on the Nyquist plot of the open-loop characteristics.

III. Magnetic-head positioning system in HDD

A. Control system

Fig. 4 shows the internal components of the HDD with its cover removed. The HDD includes a VCM (Voice Coil Motor), PZT (Lead Zirconate Titanate) actuators, an HSA (Head-Stack Assembly), magnetic heads, disks, and a spindle motor. The VCM moves the HSA radially across the disks, while the PZT actuators fine-tune the position of the magnetic heads with limited stroke. Fig. 5 shows the block diagram of the magnetic-head positioning control system used in this study. It consists of feedback controllers C_{dv} and C_{dp} for the VCM and the PZT actuator, respectively, an interpolator I_p, multi-rate filters F_{mv} and F_{mp} for the VCM and the PZT actuator, respectively, a multi-rate zero-order hold $\mathcal{H}_m$, a sampler $\mathcal{S}$,

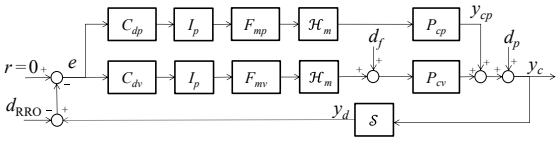

Fig. 5. Block diagram of magnetic-head positioning system.

TABLE I
VARIATIONS OF PLANT PARAMETERS IN THE BENCHMARK PROBLEM.

Case	ω_{pv}	ω_{pp}	ζ_{pv}	ζ_{pp}	K_{pp}
1	$+4\%$	$+6\%$	-20%	-20%	0%
2	0%	0%	0%	0%	0%
3	-4%	-6%	$+20\%$	$+20\%$	0%
4	$+4\%$	$+6\%$	-20%	-20%	$+5\%$
5	0%	0%	0%	0%	$+5\%$
6	-4%	-6%	$+20\%$	$+20\%$	$+5\%$
7	$+4\%$	$+6\%$	-20%	-20%	-5%
8	0%	0%	0%	0%	-5%
9	-4%	-6%	$+20\%$	$+20\%$	-5%

and the plant models P_{cv} and P_{cp} for the VCM and the PZT actuator, respectively. The interpolator I_p, which includes an up sampler and an averaging filter with the multi-rate number 2, generates the reference signal for the PZT actuator from the VCM output. In this study, the sampling time of the control system (T_s) is 1.98 [μs].

B. Benchmark problem

A technical committee of HDD servo researchers from prominent universities and a Japanese HDD manufacturer devised an open-source HDD benchmark problem [12]. Experts in this field presented their works using the HDD benchmark problem [2], [13]–[21].

1) Controlled object [22]: The ambient temperature of most HDDs ranges from 5 to 60 deg. Therefore, this benchmark problem provides two boundary samples: a low-temperature (LT) model and a high-temperature (HT) model. The nominal plant is a room-temperature (RT) model.

The LT condition increases the mechanical resonance frequencies and decreases the damping ratios of both the VCM and the PZT actuators compared to the RT condition. The VCM mechanical resonance frequency (ω_{pv}) increases by 4%, the PZT actuator mechanical resonance frequency (ω_{pp}) by 6%, and the damping ratios of both the VCM (ζ_{pv}) and the PZT actuators (ζ_{pp}) decrease by 20%.

The HT condition has the opposite effect: it decreases the mechanical resonance frequencies and increases the damping ratios of both the VCM and the PZT actuators compared to the RT condition. The VCM mechanical resonance frequency decreases by 4%, the PZT actuator mechanical resonance frequency by 6%, and the damping ratios of both the VCM and the PZT actuators increase by 20%.

The magnetic-head positioning control system also requires robustness against the gain variation of the PZT actuators. Therefore, this benchmark problem uses three parameters for the PZT actuator gain (K_{pp}) variation: -5%, 0%, and $+5\%$. As a result, this benchmark problem has nine cases

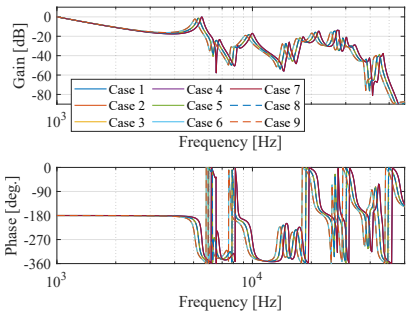

(a) P_{cv}

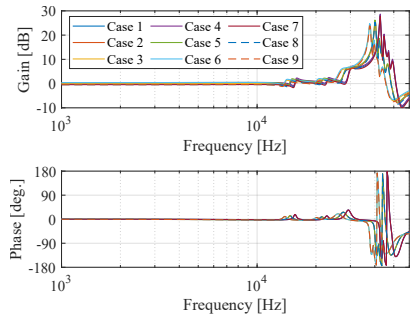

(b) P_{cp}

Fig. 6. Frequency responses of mechanical characteristics in the benchmark problem.

for the controlled object. Table I shows the variations of plant parameters from the nominal model. Fig. 6 shows the frequency responses of P_{cv} and P_{cp}.

2) Disturbance: This benchmark problem considers three disturbances for the magnetic-head positioning control system as follows:

- RV (Rotational Vibration): This is d_f in Fig. 5. It is the rotational acceleration caused by the operating HDDs next to each other, which degrades the magnetic-head positioning system.
- Fan-induced vibration: This is d_p in Fig. 5. It is the large air vibration (wind noise) produced by the cooling fans in the data center storage box, which affects the HDDs through an airborne path.
- RRO (Repeatable RunOut): This is d_{RRO} in Fig. 5. It is the residual error after the RRO compensation by the learning process in the production lines of the latest HDDs. This benchmark problem uses the d_{RRO} as measurement noise (random signal).

3) Control system with pre-set controller: This benchmark problem provides a pre-set controller as an example. Fig. 7 shows the frequency responses of the control system characteristics with the pre-set controllers: (a) Bode plot of open-loop, (b) Nyquist plot of open-loop, and (c) Gain Bode plot of sensitivity function. Fig. 8 shows the simulation results of y_c with the pre-set controllers: (a) time domain and (b) amplitude spectrum.

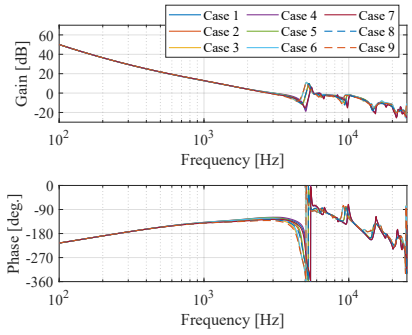

(a) Open-loop (Bode plot).

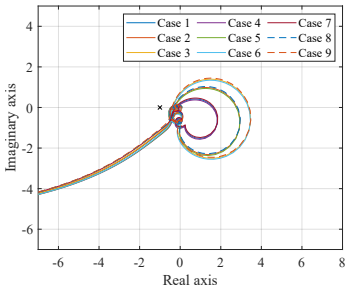

(b) Open-loop (Nyquist plot).

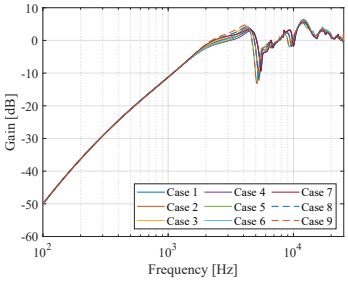

(c) Sensitivity functions.

Fig. 7. Frequency responses of the control system with the pre-set controller in the benchmark problem. The worst case of $||S||_\infty$ is 6.39 [dB].

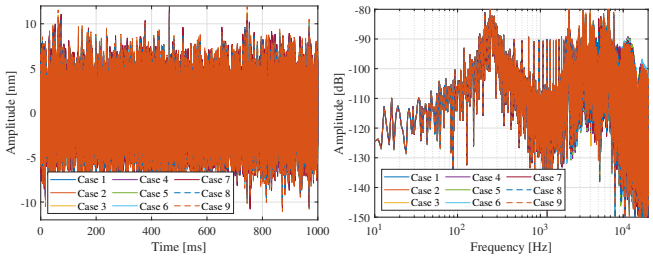

(a) Time domain (b) Frequency domain

Fig. 8. Simulation results of y_c with the pre-set controller in the benchmark problem. The worst case of $3\sigma = 14.54$ [% of track width].

IV. Control System Design with Resonant Filters

In this study, we employ a control system equipped with three types of resonant filters: R_{sv}, R_{sp}, and R_{sd}, as depicted in Fig. 9, for the HDD benchmark problem. Specifically:

- R_{sv}: This resonant filter is designed for the VCM loop and compensates for disturbances occurring below 4 kHz.

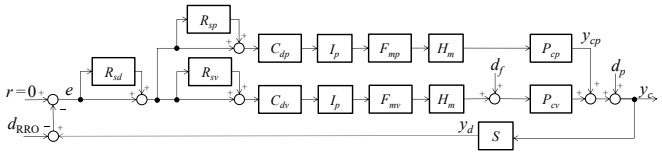

Fig. 9. Block diagram of HDD benchmark problem with the resonant filters.

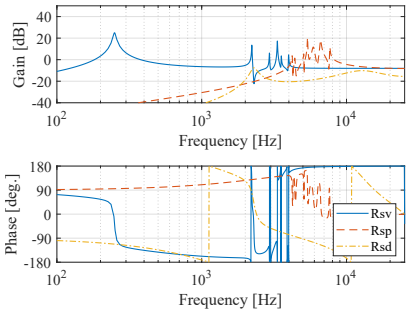

Fig. 10. Frequency responses of resonant filters using stable poles only.

- R_{sp}: The resonant filter R_{sp} is intended for the PZT loop and compensates for disturbances above 4 kHz.
- R_{sd}: This resonant filter is applied to the open-loop of the control system. It compensates for the gain degradation of the sensitivity function $|S[z]|$ caused by the use of R_{sv} or R_{sp}.

It's important to note that all controllers, except for the resonant filters, remain consistent with the pre-set control system used in the HDD benchmark problem. The resonant frequencies of R_{sv} and R_{sp} were determined based on simulation results of y_c using the pre-set controllers shown in Fig. 8 (b).

A. Using resonant filter with stable poles (conventional method)

Fig. 10 shows the frequency responses of resonant filters R_{sv} (solid), R_{sp} (dashed), and R_{sd} (dot-dashed) using stable poles only. In this case, resonances created by R_{sd} have small peak gains because R_{sd} compensate for the increased gain of $|S[z]|$ by employing R_{sv} or R_{sp}. Fig. 11 shows frequency responses of the control system ((a) Bode plot of the open-loop, (b) Nyquist plot of the open-loop, (c) Gain Bode plot of the sensitivity function). In this case, the worst case of $||S||_\infty$ is 6.38 [dB].

B. Using resonant filter with unstable poles (proposed method)

The resonant filters with the unstable poles must have large peak gain in order to contain the coordinates $[-1, 0j]$ inside the circle on the Nyquist plot of the open-loop characteristics. Therefore, we employ the unstable poles for R_{sv} only. Fig. 12 shows the frequency responses of resonant filters using unstable poles for R_{sv}. In this case, R_{sp} and R_{sd} do not employ unstable poles. Fig. 13 shows the frequency responses of the control system. In this case, the worst case of $||S||_\infty$ is 6.38 [dB].

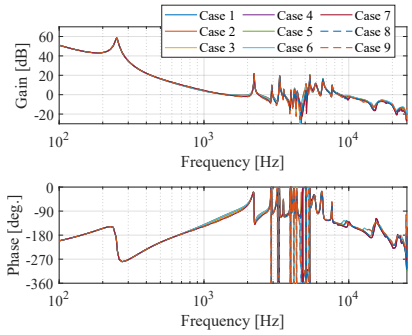

(a) Open-loop (Bode plot).

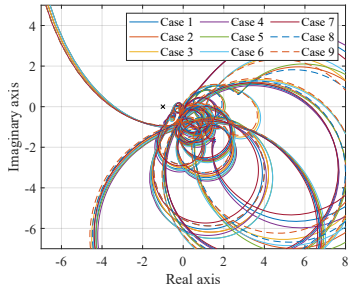

(b) Open-loop (Nyquist plot).

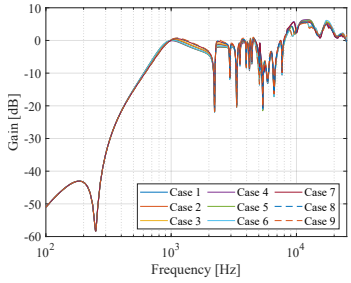

(c) Sensitivity functions.

Fig. 11. Frequency responses of the control system with resonant filters using stable poles only. The worst case of $||S||_\infty$ is 6.38 [dB].

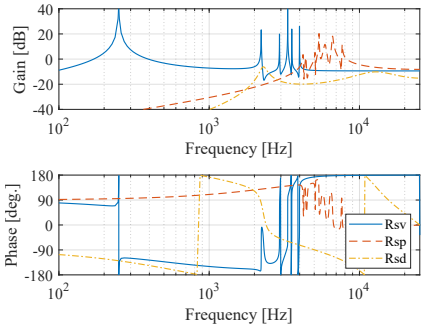

Fig. 12. Frequency responses of resonant filters using unstable poles for R_{sv}.

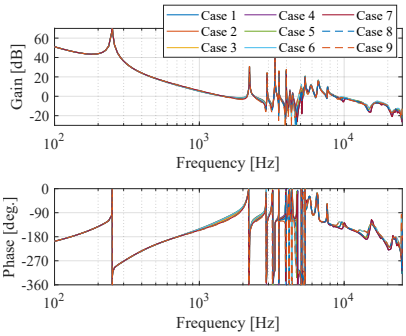

(a) Open-loop (Bode plot).

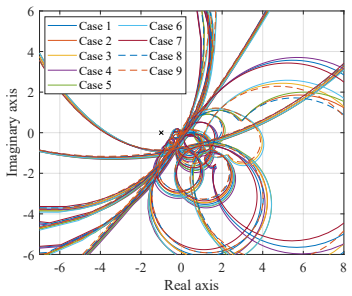

(b) Open-loop (Nyquist plot).

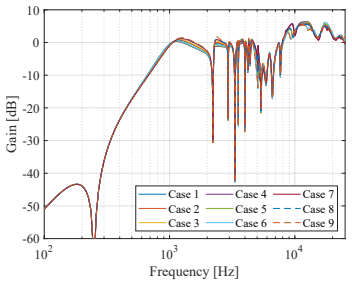

(c) Sensitivity functions.

Fig. 13. Frequency responses of the control system with resonant filters using unstable poles for R_{sv}. The worst case of $||S||_\infty$ is 6.38 [dB].

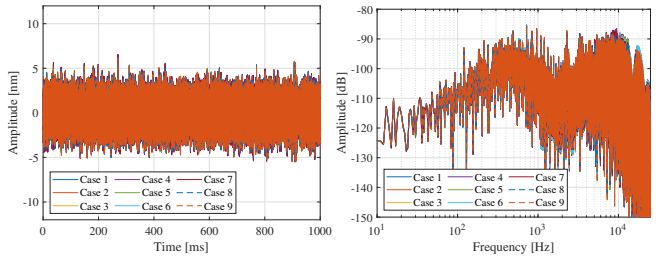

(a) Time domain (b) Frequency domain

Fig. 14. Simulation results of y_c with resonant filters using stable poles only. The worst case of $3\sigma = 7.31$ [% of track width].

V. Validation

In order to validate the proposed method, we conducted the simulations with the HDD benchmark problem. Fig. 14 shows the simulation results with results of y_c with resonant filters using stable poles only. Fig. 15 shows the simulation results with results of y_c with resonant filters using unstable poles for R_{sv}. In both figures, (a) indicates the time domain characteristics, (b) indicates the frequency domain characteristics (amplitude spectrum).

In Fig. 16 (a), we present a comparison of the 3σ values for y_c between the results with the loop-shaping method with resonant filters and the result with the pre-set controller. The

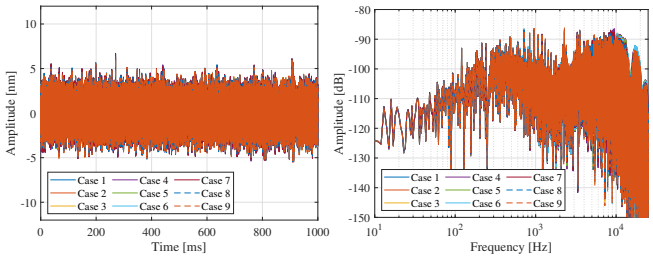

(a) Time domain (b) Frequency domain

Fig. 15. Simulation results of y_c with resonant filters using unstable poles for R_{sv}. The worst case of $3\sigma = 7.27$ [% of track width].

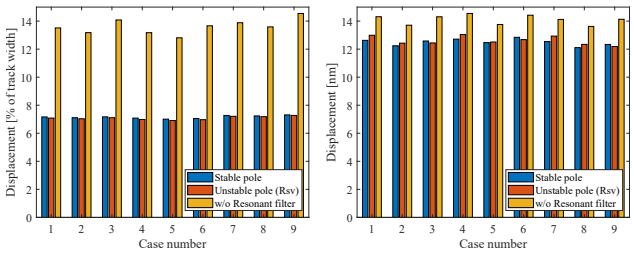

(a) 3σ value of y_c (b) Maximum value of y_{cp}

Fig. 16. Comparison results of y_c and y_{cp}

results clearly demonstrate that loop-shaping methods with the stable poles only improve the positioning accuracy without losing the stability margins. Moreover, employing the resonant filters with the unstable poles for R_{sv} enables us to improve the positioning accuracy as much as the resonant filters with the stable poles.

In Fig. 16 (b), we present a comparison of the maximum values for y_{cp} between the results with the loop-shaping method with resonant filters and the result with the pre-set controller. This figure shows that our proposed method enables us to improve the positioning accuracy without increasing the strokes of the PZT actuators.

VI. Conclusion

In order to compensate for the disturbances beyond the servo bandwidth for the magnetic-head positioning system in HDDs, we have proposed the loop-shaping method that incorporates unstable poles. The proposed method involves introducing unstable poles instead of the conventional stable poles for the resonance filter used in loop shaping which enables us to decrease the gain of the sensitivity functions at disturbance frequencies. Validation results using the HDD benchmark problem demonstrate that our proposed methods effectively reject disturbances in the high-frequency range while maintaining robust performance without increasing the strokes of the PZT actuators.

References

[1] T. Atsumi, A. Okuyama, and M. Kobayashi, "Track-Following Control Using Resonant Filter in Hard Disk Drives," *The IEEE/ASME Transactions on Mechatronics*, vol. 12, no. 4, pp. 472–479, 2007.

[2] M. Mae, W. Ohnishi, and H. Fujimoto, "Frequency Response Data-Based Resonant Filter Design Considering Phase Stabilization and Stroke Limitation Applied to Dual-Stage Actuator Hard Disk Drives," in *The 22nd IFAC World Congress 2023*, pp. 11 390–11 395, 2023.

[3] Y. W. Jeong and C. C. Chung, "Observer-based Robust Control: Its Application to Permanent Magnet Synchronous Motors," *IEEJ Journal of Industry Applications*, vol. 12, no. 4, pp. 575–587, 2023.

[4] R. A. B. Petrea, R. Oboe, and G. Michieletto, "Safe High Stiffness Impedance Control for Series Elastic Actuators using Collocated Position Feedback," *IEEJ Journal of Industry Applications*, vol. 12, no. 4, pp. 735–744, 2023.

[5] T. T. Phuong, K. Ohishi, and Y. Yokokura, "High-Performance Sensorless Force Control Using Superior Wideband and Periodicity-Cancellation Force Observer," *IEEJ Journal of Industry Applications*, vol. 12, no. 4, pp. 773–785, 2023.

[6] T. Atsumi and S. Yabui, "Loop-Shaping Technique for Quadruple-Stage Actuator System in Hard Disk Drive," *IEEE Transactions on Industry Applications*, vol. 59, no. 4, pp. 5009–5018, 2023.

[7] R. Kitayoshi, Y. Yoshiura, and Y. Kaku, "Σ-X Series: AC Servo Drive for Achievement of Digital Solution," *IEEJ Journal of Industry Applications*, vol. 12, no. 5, pp. 859–867, 2023.

[8] M. Takeuchi and S. Katsura, "Robust Velocity Control for Electromagnetic Friction Brake Based on Disturbance Observer," *IEEJ Journal of Industry Applications*, vol. 12, no. 5, pp. 876–884, 2023.

[9] S. Nagao, Y. Kawai, Y. Yokokura, K. Ohishi, and T. Miyazaki, "Load-side Acceleration Control Based on Single Inertialization Compensator and Jerk Observer for Industrial Robots," *IEEJ Journal of Industry Applications*, vol. 12, no. 6, pp. 1034–1045, 2023.

[10] Y. Tsuji, D. Yashiro, Y. Kato, S. Bando, K. Yubai, and S. Komada, "Design of a Thrust Controller for Propeller Driven Systems Operating at Multiple Wind Velocities and Propeller Angular Velocities," *IEEJ Journal of Industry Applications*, vol. 12, no. 6, pp. 1060–1067, 2023.

[11] K. Miyata, S. Hara, K. Hayashi, K. Seki, M. Iwasaki, and M. Otsuki, "Vision-Based Target Tracking Controller Design for Asteroid Flyby Problem," *IEEJ Journal of Industry Applications*, vol. 12, no. 5, pp. 914–923, 2023.

[12] T. Atsumi, "Benchmark Problem for Magnetic-Head Positioning Control System in HDDs," in *The 22nd IFAC World Congress 2023*, pp. 9484–9490, 2023.

[13] S. Yabui, T. Atsumi, and A. Okuyama, "Control Scheme of RRO Compensation for Track Mis-Registration in HDDs," in *The 22nd IFAC World Congress 2023*, pp. 6905–6910, 2023.

[14] S. Bashash, "Automated Multi-Objective Control Optimization of Dual-Stage Hard Disk Drive Servo Systems," in *The 22nd IFAC World Congress 2023*, pp. 11 402–11 405, 2023.

[15] X. Wang, W. Ohnishi, and T. Atsumi, "Systematic Filter Design by Convex Optimization for Disturbance Rejection in Dual-Stage Actuated Hard Disk Drives," in *The 22nd IFAC World Congress 2023*, pp. 11 384–11 389, 2023.

[16] M. Hirata, J. Shimokasa, and M. Suzuki, "Two-Step Design of H-Inifinity Controller for Dual Stage Hard Disk Drives," in *The 22nd IFAC World Congress 2023*, pp. 11 376–11 379, 2023.

[17] N. Potu Surya Prakash, J. Seo, A. Rose, and R. Horowitz, "Data-Driven Track Following Control for Dual Stage-Actuator Hard Disk Drives," in *The 22nd IFAC World Congress 2023*, pp. 11 380–11 383, 2023.

[18] R. Muto and Y. Uchimura, "Controller Design for HDD Benchmark Problem Using RNN-Based Reinforcement Learning," in *The 22nd IFAC World Congress 2023*, pp. 4830–4835, 2023.

[19] R. J. Caverly, M. Chakraborty, B. Huang, and R. Sosseh, "Robust Mixed H_2-H_∞ Control Synthesis for Dual-Stage Hard Disk Drives Using Convex Optimization," in *The 22nd IFAC World Congress 2023*, pp. 11 396–11 401, 2023.

[20] J. Ouyang and X. Chen, "A Recursive System Identification With Non-Uniform Temporal Feedback Under Coprime Collaborative Sensing1," *ASME Letters in Dynamic Systems and Control*, vol. 3, no. 2, p. 021010, 2023.

[21] T. Atsumi, S. Yabui, and S. Nakadai, "Optimization Method for Magnetic-Head Positioning Control System in HDD Against Unexpected Plant Perturbations by Using Data Mining Techniques," *IEEE Transactions on Magnetics*, vol. 60, no. 1, pp. 1–14, 2024.

[22] T. Atsumi and S. Yabui, "Quadruple-Stage Actuator System for Magnetic-Head Positioning System in HDDs," *The IEEE Transactions on Industrial Electronics*, vol. 67, no. 11, pp. 9184–9194, 2020.